Assessing the Global Relationships Between Teleconnection Factors and Terrestrial Water Storage Components

Peijun Li[1], Yuanyuan Zha[1], Liangsheng Shi[1], Hua Zhong[1], Chak-Hau Michael Tso[2,3] & Mousong Wu[4,5]

Postprint for:

Li, P., Zha, Y., Shi, L. *et al.* Assessing the Global Relationships Between Teleconnection Factors and Terrestrial Water Storage Components. *Water Resour Manage* **36,** 119–133 (2022). https://doi.org/10.1007/s11269-021-03015-x

[1]State Key Laboratory of Water Resources and Hydropower Engineering Science, Wuhan University, Wuhan, Hubei 430072, China
[2]Lancaster Environment Centre, Lancaster University, Lancaster, UK
[3]UK Centre for Ecology and Hydrology, Lancaster, UK
[4]International Institute for Earth System Science, Nanjing University, Nanjing, Jiangsu 210023, China
[5]Jiangsu Provincial Key Laboratory of Geographic Information Science and Technology, Key Laboratory for Land Satellite Remote Sensing Applications of Ministry of Natural Resources, School of Geography and Ocean Science, Nanjing University, Nanjing, Jiangsu 210023, China

Abstract

It has been shown that the changes in global terrestrial water storage (TWS) are strongly linked to the teleconnections (TCs) that induce large-scale climate variations. However, the contributions of the different TCs to global changes of TWS and its components (water storage components, WSCs) remain undetermined. To fill this gap, we systematically assess the relationships between six major ocean-related TCs and different WSCs derived from the Gravity Recovery and Climate Experiment (GRACE) mission and hydrological models under different timescales. Additionally, the interrelationships of the TCs are also analyzed via the independent component analysis for further investigation. The results allow an improved understanding of the hydrometeorological process controlling WSC changes. Specifically, the annual timescale analysis can constrain high-frequency noises and retain the informative fluctuations of WSC residuals. ENSO and AMO are found to be the two most dominant TCs controlling the variations of WSCs globally. TWS and groundwater storage (GWS) are the two WSCs most correlated with the dominant TCs. The WSCs at shallow depths, which are largely affected by strongly hysteretic controls of TCs, are more closely linked to the TCs with many high-frequency components that tend to have weak hysteresis on WSCs. As for the interrelationships of TCs, the independent component, which is highly correlated with all six TCs, has a predominant influence on WSCs.

Introduction

As a fundamental component of the terrestrial hydrological cycle, terrestrial water storage (TWS) includes many subcomponents like water in lakes, soil, and aquifers (Scanlon et al. 2018). The inter-annual and decadal climate variability caused by large-scale ocean-atmosphere teleconnections (TCs) is an overwhelming non-negligible factor affecting regional water resources, modulating the location and strength of storm tracks and fluxes of heat, moisture, and momentum (Chen et al. 2021b; Ni et al. 2018; Oñate-Valdivieso et al. 2020). The changes in TWS and its components (water storage components, WSC) due to TCs have important implications for assessing climate variability, food security, water and energy use, and drought/flood risk (Guo et al. 2019).

Traditional estimation of TWS change has been mainly conducted in two ways (Ni et al. 2018): using the water balance method and summing all WSCs. It is a cumbersome process, requiring large observational data or sophisticated models (Han et al. 2019). Alternatively, the Gravity Recovery and Climate Experiment (GRACE) has provided unprecedented global TWS change observations since its launch in 2002. With improved data quality and more than a decade of observations, GRACE TWS has been widely used for assessing the impacts of climate change on regional and global water resources as well as carbon cycle (Banerjee and Kumar 2018; Nie et al. 2018; Humphrey et al. 2018; Thomas and Famiglietti 2019).

Many studies have analyzed the relationships between GRACE TWS and TCs. The impacts of TCs on TWS changes in specific regions (e.g., Yunnan Province (Han et al. 2019)), river basins (e.g., major Indian river basins (Soni and Syed 2015), Yangtze River (Zhang et al. 2015)) and types of river basins (e.g., endorheic basins (Wang et al. 2018)) have been studied. However, a regional evaluation may experience bias in calculating the region-averaged TWS when different drying and wetting trends exist in a given region (Liu et al. 2020; Sun et al. 2018). Besides, previous studies examined TWS dynamics at specific time scales (Liu et al. 2020; Phillips et al. 2012), which may be affected by the high-frequency noise in the dynamics and ignoring the various performances over multiple-time scales. As for the grid-based or site-based analyses, many studies only focused on single TC globally (e.g., grid-based analysis for El Niño–Southern Oscillation (ENSO) (Ni et al. 2018; Phillips et al. 2012)) or some TCs regionally (e.g., grid-based studies in Australia (García-García et al. 2011), West Africa (Ndehedehe et al. 2017) and the Asian and eastern European regions (Liu et al. 2020) and Africa (Anyah et al. 2018)). To the best of our knowledge, only Guo et al. (2021) investigated the relationships between global TWS and multiple TCs. However, it remain unclear which WSCs are most correlated with the dominant TCs. The impacts of more TC factors on global WSCs need to be comprehensively analyzed due to the differences in their properties and interrelationships of TCs and WSCs, which would be helpful for understanding and predicting water resource changes (Kennedy et al. 2009). When considering the relationships between TCs and WSCs, direct or trend-remained cross-correlation analyses are often used (Anyah et al. 2018; Han et al. 2019; Soni and Syed 2015). However, the results may be affected by human activity and long-term climate change since they contribute to the change in trends instead of

interannual climate variability (Liu et al. 2020; Phillips et al. 2012; Scanlon et al. 2016; Wang et al. 2018).

The main novelty of our study is to fill the gap of existing research via the use of several signal processing methods to suppress the irrelevant factors and identify the unique relationships between the different hydrological WSCs and TCs for a better understanding of large-scale hydrometeorological processes. To this end, the study decomposes the different WSC time series derived from GRACE observations and model simulations via the Seasonal-Trend Decomposition by Loess (STL) method. We systematically examine the influences of TC factors on WSC residuals by considering multiple ocean-related TC factors (i.e., North Atlantic Oscillation (NAO), Atlantic Multidecadal Oscillation (AMO), ENSO, Pacific Decadal Oscillation (PDO), Arctic Oscillation (AO), Indian Ocean Dipole (IOD)) and determine possible dominant TCs and WSCs most correlated with the dominant TCs. Additionally, their relationships under different time scales via the moving-average method are investigated to find the best appropriate data processing. Subsequently, a higher-order statistical method of independent component analysis (ICA (Anyah et al. 2018)) is applied to filter the interrelationships among the six TCs and isolate any unique or combined influences of these indices on WSCs (e.g., ENSO and PDO (Girishkumar et al. 2015)), which is helpful for us to identify unique regions strongly affected by such relationships (Anyah et al. 2018).

In the following sections, we first describe the datasets used in Sect. 2. The methods and data processing steps are described next in Sect. 3. We then exhibit the results in Sect. 4. The uncertainties and limitations of this study are discussed in Sect. 5. The conclusions are finally summarized in Sect. 6.

Datasets

Six WSC datasets and six major ocean-related TCs are used in the study. Table 1 lists the types and sources of data used. Their detailed information is described below. We exclude the contribution of Antarctica since it is not included in the hydrological and land surface model outputs.

Table 1 List of the main data sets used in this study

Data type	Data source
Water storage component:	
TWS	JPL RL06 mascon v2
SWS	WGHM v2.2d
SnWS	CLSM 2.1 and WGHM v2.2d
PCW	CLSM 2.1 and WGHM v2.2d
RZSM	CLSM 2.1 and WGHM v2.2d
GWS	CLSM 2.1 and WGHM v2.2d
Teleconnection:	

NAO	NOAA
ENSO	NOAA
PDO	NOAA
AO	NOAA
AMO	NOAA
IOD	NOAA

*The above Acronyms can refer to List of Acronyms.

GRACE-derived Terrestrial Water Storage (TWS)

The RL06 GRACE monthly solutions based on regional mass concentration (mascon) functions provided by the Jet Propulsion Laboratory (JPL), USA with 0.5° resolution are used in this study, as in Sun et al. (2020). Scanlon et al. (2016) suggested that the performance of GRACE mascons in 176 global basins is not worse than traditional-scaled spherical harmonics. Capturing all the signals observed by GRACE within the measurement noise level, TWS is given in equivalent water thickness. The study period is between April 2002 and December 2016 (i.e., 177 epochs with a linear interception (Liu et al. 2020; Long et al. 2015; Yang et al. 2017)).

Other Water Storage Components (WSCs) From Model Outputs

The WaterGAP Global Hydrology Model (WGHM, v2.2d) (Müller Schmied et al. 2020) simulates many kinds of WSCs (e.g., surface, soil and groundwater) and considers some anthropogenic influences (e.g., human water use) on them. WGHM has a qualitatively reasonable performance to describe global-scale water resources (Hu et al. 2021). As a kind of GLDAS-2.1 product, the catchment land surface model (CLSM) simulates the shallow groundwater and has been upgraded by initializing soil moisture over desert (Xia et al. 2019). In this study, we use WGHM (0.5 degree and one month) to derive the surface water storage (SWS) and use CLSM (1 degree and one month) and WGHM to derive snow water storage (SnWS), plant canopy water (PCW), root zone soil moisture (RZSM) and groundwater storage (GWS), as in Hu et al. (2021).

Teleconnections (TCs)

In this work, we use six important atmosphere-ocean coupled TCs, including ENSO, NAO, AMO, AO, PDO and IOD. They characterize patterns of coupled atmosphere-ocean variability in different anomaly centers and may be modulated by each other (Girishkumar et al. 2015; Guo et al. 2021; Saji and Yamagata 2003). Their detailed information is described in the Supplementary Material.

Methods

The methodology flow diagram in Fig. 1 exhibits the primary steps of data processing. First, we derived different WSCs (i.e., TWS, SWS, SnWS, PCW, RZSM and GWS) from different sources (i.e., GRACE JPL RL06 mascon, WGHM and CLSM) with a consistent temporal-spatial resolution (i.e., 0.5 degree and one month) via the linear interpolation and resampling methods. Second, the residuals of WSCs are obtained via the STL method. Third, the residuals are filtered via the moving average method for multi-timescale analyses. Fourth, we conduct the cross-correlation analyses between the residuals and TCs as well as their independent components (ICs) via the ICA method. The main methods used are described below.

Fig. 1

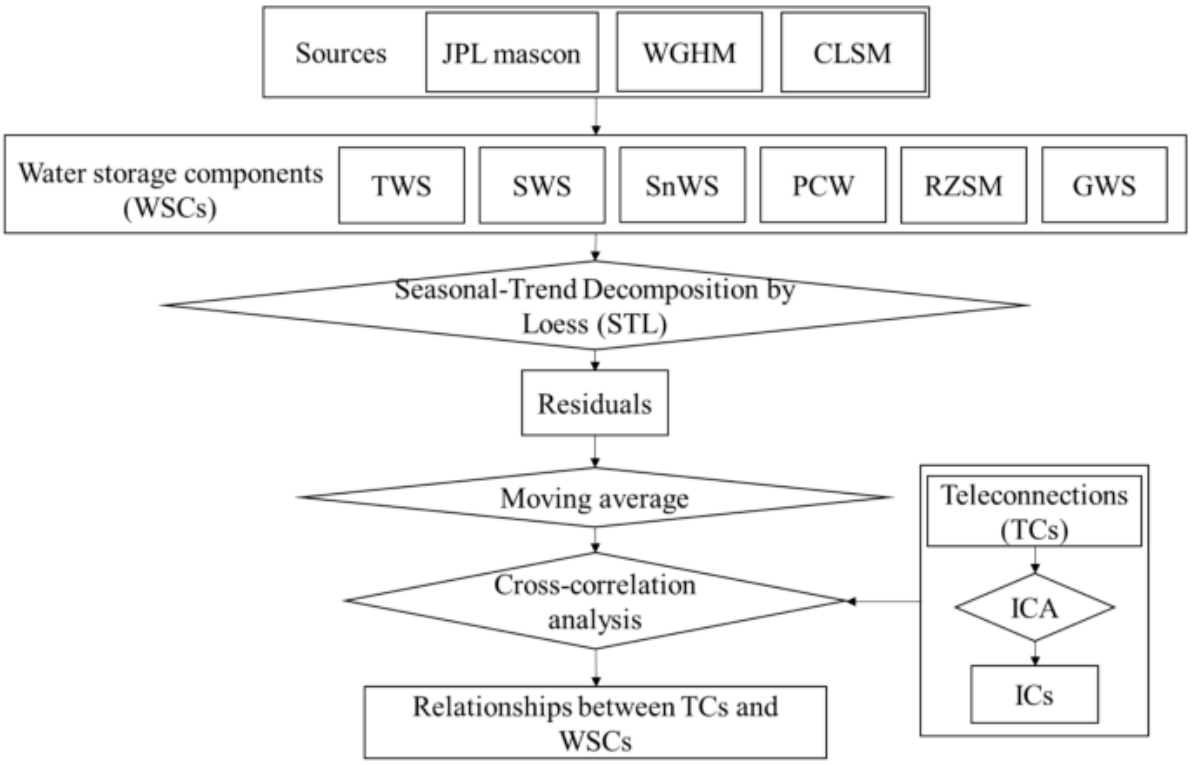

Methodology flowchart of data processing in this study

Time Series Decomposition: Seasonal-trend Decomposition by Loess (STL) Method

We decompose an original WSC signal into three parts: a long-term trend, a seasonal component, and a residual component via the STL approach (Cleveland et al. 1990), which is a robust method to decompose time series and can be described as follows:

$$S_{sum} = S_{trend} + S_{seasonal} + RE \quad (1)$$

where S_{sum}, S_{trend}, $S_{seasonal}$ and RE represent the original time series, the long-term trend, the seasonal and residual components. The setting of necessary parameters in this study can be found in the Supplementary Material.

Independent Component Analysis

The ICA technique (Hyvärinen et al. 2001) uses the higher-order statistical indicators (higher than second-order mutual statistical information, e.g., principal component analysis) to extract modes that are statistically mutually as independent as possible from TCs.

In the ICA model, the data matrix **O** ($M\times E$) of the raw TCs is assumed to be a linear combination of some unknown latent variables represented as the original signal matrix **S** ($P\times E$), which can be shown as,

$$\mathbf{O} = \mathbf{AS} \tag{2}$$

where the mixing matrix **A** ($M\times P$) describes the linear transformation from **S** to **O**, M denotes the number of raw TCs, E is the number of epochs, P is the number of the derived latent source signal. Each IC ($1\times E$) in the original signal matrix **S** has its weight vector **a** ($M\times 1$) in the mixing matrix **A**. The original signals can be derived via the inverse of the mixing matrix **A** (i.e., the unmixing matrix **W** ($P\times M$)). It is the key step to find such **A** or **W** to generate original signals as statistically independent as possible. In this study, the ICA algorithm proposed by Hyvärinen and Oja (2000) is used.

Cross-correlation Analysis

In this study, we analyze the cross-correlation between the WSC residuals and TCs with the consideration of time lag since climate changes generally lead to hydrological changes (Liu et al. 2020). The cross-correlation measures the strength and direction of a linear relationship between the two time series, and it has been used in many hydrology studies (e.g., Krishan et al. (2014)). The correlation coefficient can be calculated as follows:

$$r(\tau)=\frac{Var_{12}(\tau)}{\sqrt{Var_{11}Var_{22}}} \tag{3}$$

where $Var_{12}(\tau)$ is the covariance between the leading TC and the lagging WSC, τ is the lag, and $Var_{11}(\tau)$ and $Var_{22}(\tau)$represent the variances of TC and WSC, respectively. Only the historical and current influence of TCs on the WSC residuals are considered; therefore, the values of lag τ range between 0 and 24 months (Liu et al. 2020; Ni et al. 2018). In each study site, we calculate the correlation between the different combinations of TCs and WSCs. The TC and WSC with the maximum absolute value are termed as the dominant TC and the dominant WSC, respectively.

Results

Relationships Under Different Timescales Via Moving Average

Figure 2 shows that the modes of distributions of maximum correlation coefficients gradually go away from the y-axis as the size of the moving average window increases. However, the

amplitudes of the increase are large between 1 month and 12 months and become small between 12 months and 60 months. The high-frequency noises of a time series can be filtered out via moving average, while moving average with excessively large sliding periods can result in over smoothed data since the relatively high-frequency components that include valuable information may get lost. Therefore, a moving average with a 12-month window is selected for this study.

Spatial Patterns of Links Between TCs and WSCs

The spatial distributions of cross-correlation analyses between TCs and WSCs are shown in Fig. 3a–d. The corresponding basin-average results can be found in Fig. S1 of the Supplementary Material. The general spatial patterns at the basin scale are similar, especially at low latitudes. However, some spatial heterogeneities in the sub-basins are overlooked in the basin-average analyses. Besides, the areas of the dominant SnWS mainly distribute in the Northern Hemisphere. The areas of the dominant TWS and GWS mainly exist in the low- and mid-latitude (i.e., 40° to -40°) (Fig. 3a). The dominant ENSO and AMO are distributed in wide areas. The negative relationships are mainly distributed in the northern part of South America, southern Africa, and western Europe. The positive correlations are mainly distributed in North America, the southern part of South America, northern Africa, and a major part of Asia (Fig. 3d).

Fig. 2

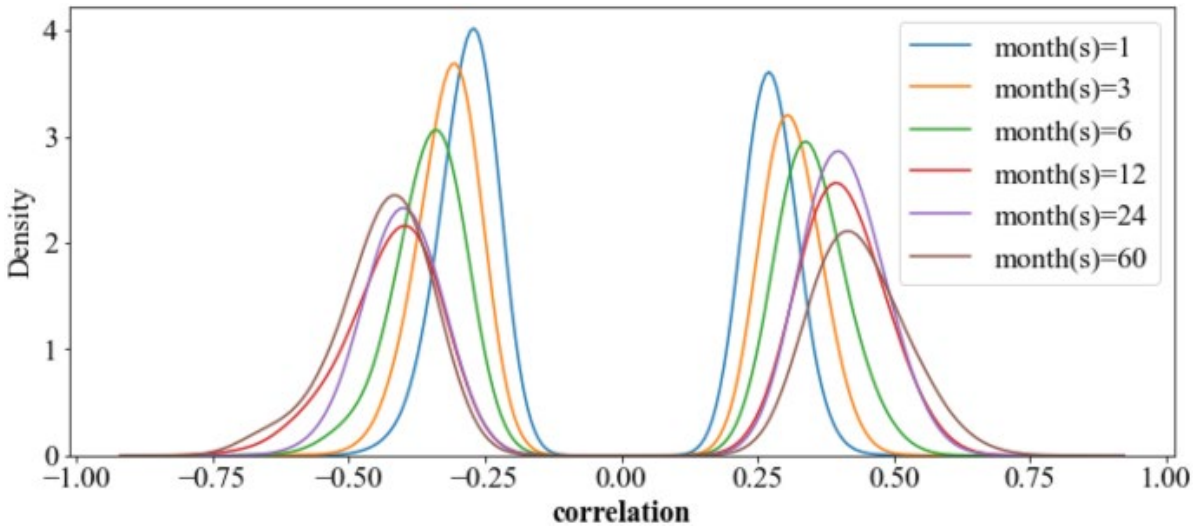

The probability distributions of maximum correlation coefficients via different months of moving average

Fig. 3

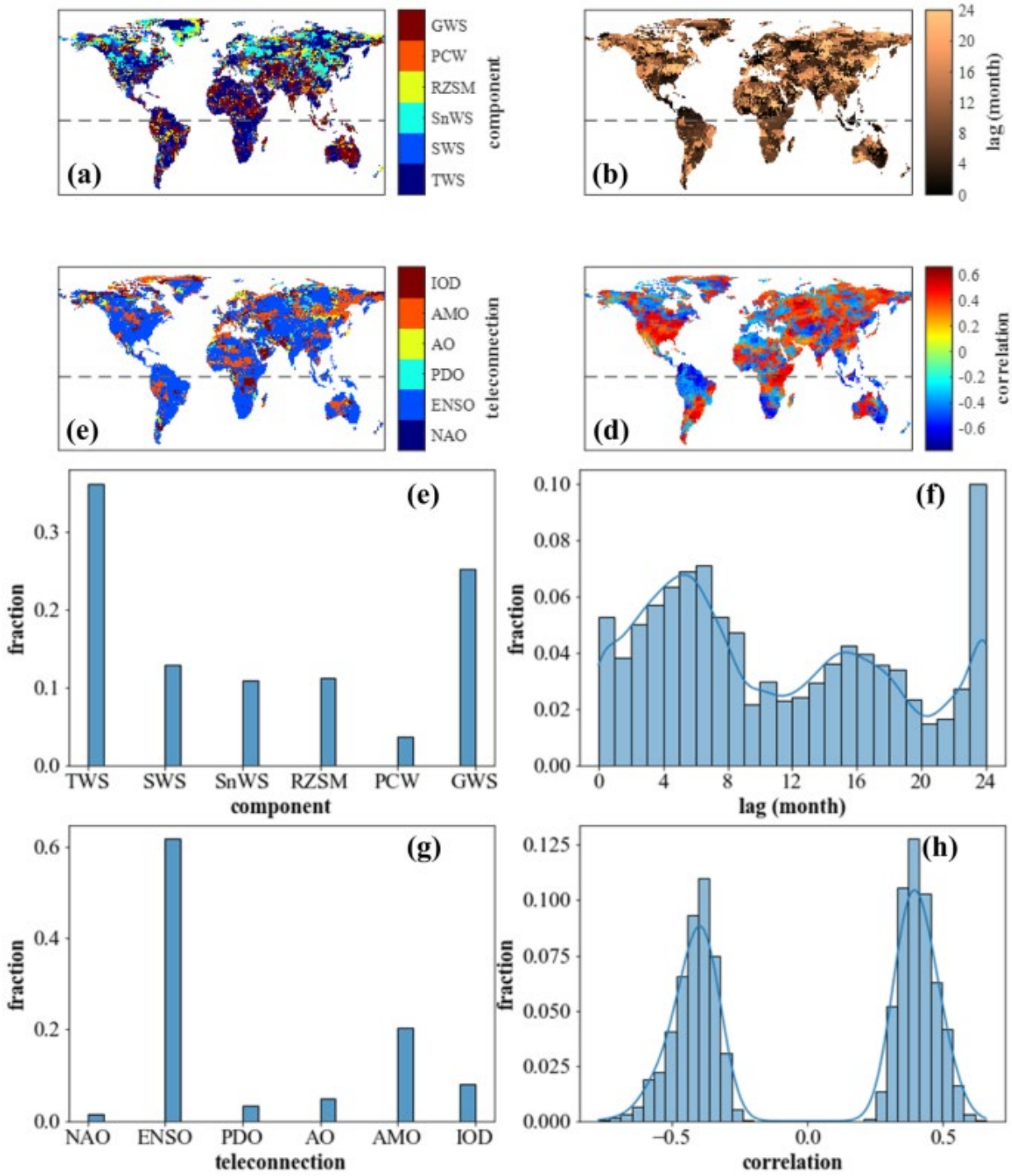

Cross-correlation analyses between TCs and WSCs: Spatial patterns of (**a**) dominant WSC; (**b**) TC lags; (**c**) dominant TC; (**d**) maximum correlation coefficients (significant threshold: $|r|>\sim 0.15$ given $p < 0.05$) and the fractions of grids of (**e**) dominant WSCs; (**f**) lags; (**g**) dominant TCs and (**h**) maximum correlation coefficients. The gray dashed line in (**a**)~(**d**) denotes the Equator

Statistical Results of the Cross-correlation Analyses

The statistical results of the cross-correlation analyses are shown in Fig. 3e–h. The two dominant WSCs are TWS and GWS, which account for 36.06% and 25.13% of the total dominant WSC distribution, respectively. The lag distribution is concentrated around five months. The two most dominant TCs are ENSO and AMO (i.e., 61.65% and 20.46%), especially for ENSO, which is also consistent with maximum absolute correlation coefficient averages among different TCs (i.e., ENSO (r=0.44), AMO (r=0.39)). Besides, in general, more significant negative correlation coefficients (i.e., r=-0.4219 and 0.4060 for negative and positive correlation coefficients, respectively) are found.

For the lag analyses, the most significant relationships between TCs and WSCs in many areas have the 24-month lag (Fig. 3b). It is reasonable since many potential larger lags (greater than 24 months) in the cross-correlation analyses may be included in the 24-month lag. It is expected that a 24-month lag can be further divided into subgroups if we are interested. The following analysis in detail similar results also confirms this point.

To further investigate the relationships between WSCs and TCs, we reanalyze the results in Fig. 3e-g. Fractions of grids of the dominant WSCs under different dominant TCs are shown in Fig. S4a. Based on Fig. S4a, SWS is most affected by NAO (i.e., 29.71%, 13.34%, 12.70%, 15.63%, 10.35% and 11.49% for NAO, ENSO, PDO, AO, AMO, IOD, respectively), which is not revealed in the general characteristics presented in Fig. 3g. Among the different dominant TCs, AMO, PDO and ENSO generally have higher fractions that strongly affect TWS and GWS. In contrast, NAO, IOD and AO generally have higher fractions that dominate SWS, PCW and RZSM. Figure S3 shows that NAO, AO, and IOD have more high-frequency components than ENSO, AMO and PDO. In addition, from SWS, PCW, RZSM to GWS/TWS, the average depths of WSCs generally increase. It exhibits a certain correlation between the depths of the dominant WSCs and the frequency components of the dominant TCs. However, the performance is not consistent for SnWS that has a relatively shallow depth. It indicates the influences of other factors like locations of anomaly centers of TCs since areas of the dominant SnWS are mainly in the Northern Hemisphere.

Like Fig. 3f, the lag distributions of different groups generally have two prominent modes (Fig. S4b–m). Figure S4b–g shows the lag distributions under different dominant TCs. The central tendencies of lag distributions of the dominant ENSO, AO, IOD, NAO are smaller, while the dominant PDO and AMO have larger central tendencies, especially for PDO. It indicates that the lags are related to the frequency components of TCs to some degree, considering that the TCs in the former have more high-frequency components than the latter.

Figure S4h–m shows that the lag distributions of dominant TWS and GWS are mainly concentrated at relatively small number of months, while other WSCs have higher fractions of large lags. The dominant WSCs at relatively shallow depths (i.e., SWS, SnWS, RZSM, PCW) are dominated by many large-lag controls from TCs since they are susceptible to TCs and hence can retain long-lasting influences of TCs suffering from the amplitude decay due to the long-

distance transmission. The small fractions of areas of the dominant SWS, SnWS, RZSM and PCW in Fig. 3e could be caused mainly by their relatively small or unstable storage values.

Influence of Independent Components of TCs Indices on WSCs

The ICA technique is applied to the TCs in order to explore the potential links between WSCs and specific or combined global TCs (as in Anyah et al. 2018) and to avoid the influence of the interdependencies among multiple TCs (Liu et al. 2020; Runge et al. 2019), e.g., ENSO and PDO (Girishkumar et al. 2015), AO and NAO (Guo et al. 2021). The time series of the four leading independent components (ICs) are retained (the details of processing is given in the Supplementary Material), which are highly related with ENSO and PDO (ENSO+PDO), NAO and AO and AMO (NAO+AO+AMO), IOD, all TCs (COMMON), respectively. The results demonstrate the uniqueness of IOD and the existence of some interdependency among the different TCs.

Figure 4a–d shows the spatial patterns of dominant WSCs, lags, and correlations via ICA. They are similar to those obtained from direct cross-correlation analysis (Fig. 3a–d), which demonstrates the robustness of the results about response of WSCs to TCs. As for the spatial distribution of the dominant TC ICs, the dominant COMMON-related IC covers the largest areas, indicating the significant influence of the common feature of the six TCs. Other TC ICs also perform significantly different spatial patterns (e.g., the wide areas dominated by the IOD-related IC). The results reveal the unique properties of TC ICs.

Compared with the statistical results in Figs. 3e–h and 4e–h exhibits similar results of the dominant WSCs (i.e., 33.64% and 23.51% for TWS and GWS, respectively). However, the second peak corresponds to a larger lag (at around 16 months) and a greater fraction, indicating stronger hysteresis via TC ICs. In addition, a slightly higher occurrence of negative correlation is also found (i.e., 51.78% for TC ICs and 47.26% for TCs). Significant differences between the results for TC ICs and TCs exist in the dominant TC-related variables. The dominant COMMON affects the greatest fraction of areas (i.e., 65.34%), while the dominant ENSO+PDO affects the least fraction of areas (i.e., 2.79%). Compared with the large areas of the dominant ENSO in Fig. 3c, g, it further demonstrates the unique properties of interrelationships of TCs and significant influences from the common feature of all six TCs on WSCs.

Fig. 4

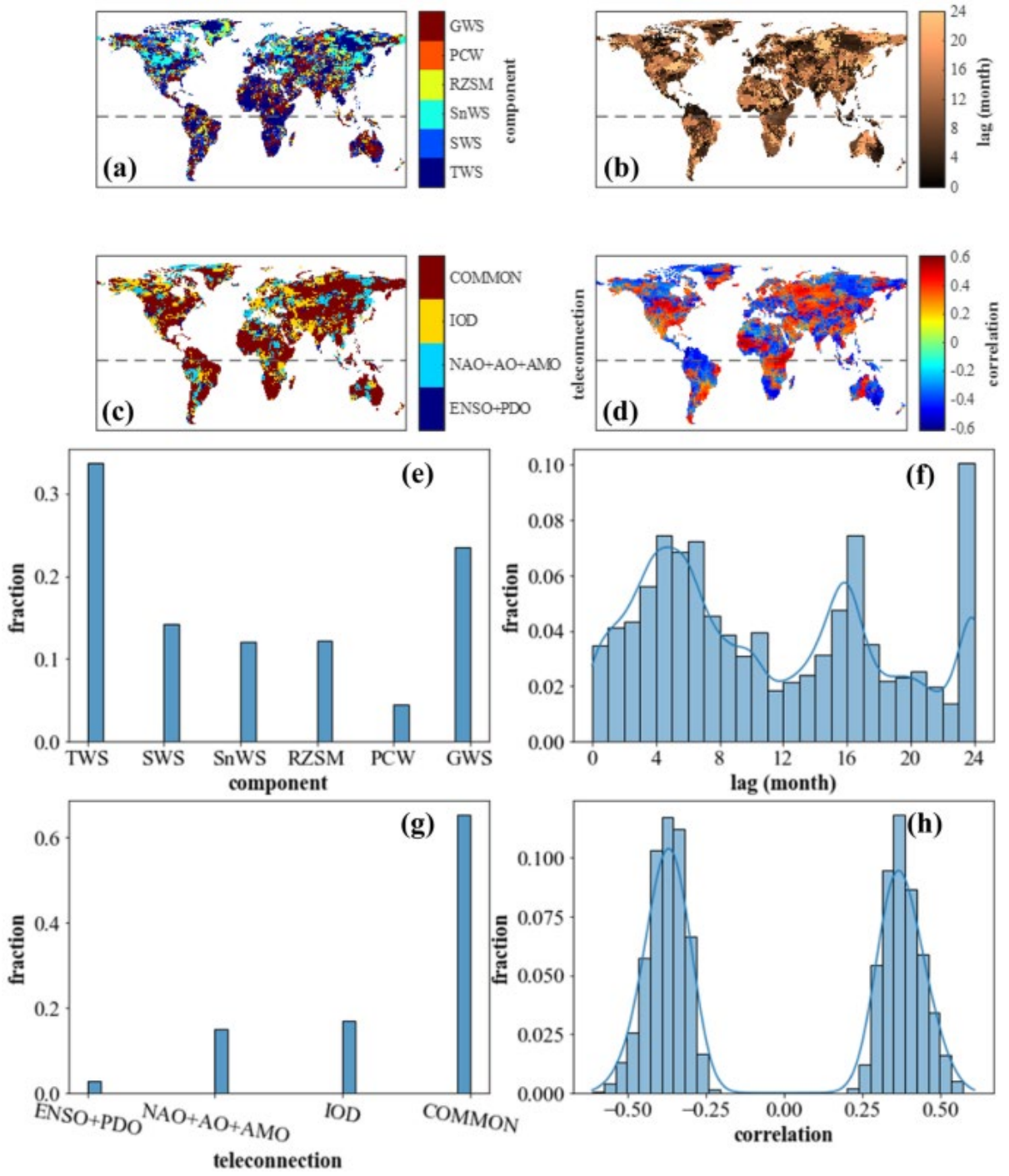

Cross-correlation analyses between between the independent components (ICs) of TCs and WSCs: spatial patterns of (**a**) dominant WSCs; (**b**) time lags; (**c**) dominant TC ICs; (**d**) maximum correlation coefficients (significant threshold: $|r|>\sim 0.15$ given $p = 0.05$) and the fractions of grids of (**a**) dominant WSCs; (**b**) lags; (**c**) dominant TC ICs and (**d**) maximum correlation coefficients. The gray dashed line in (**a**)~(**d**) denotes the Equator

Discussion

Results Compared with Previous Studies

The results presented herein have some similarities to the findings given in previous reports. The areas near the Equator (known as the intertropical convergence zone (ITCZ)) have strong maximum absolute correlation coefficients and weak lags (Ni et al. 2018). The dominant ENSO exists over large areas, e.g., Amazon Basin (Ni et al. 2018; Phillips et al. 2012), major India river basins (Soni and Syed 2015) and Yangtze River Basin (Zhang et al. 2015). There are also many areas dominated by AMO, like parts of China (Qian et al. 2014), West Africa (Ndehedehe et al. 2017), the middle of Australia, western South America (i.e., western Amazon Basin (Guo et al. 2021)). Significant spatial heterogeneity of the maximum correlation coefficients is found. Many IOD-dominated areas are distributed in the Indian Ocean rim regions where significant precipitation and temperature variability is related to IOD (Saji and Yamagata 2003). More negative correlations exist in tropical regions and Southern Hemisphere, similar to the report by Phillips et al. (2012) that there are strong negative correlations between TWS and ENSO. Besides, large fractions of areas with negative correlations are dominated by ENSO in Australia, which is consistent with Chen et al. (2021a) that reports strong La Niña induced Australia-wide wetting. Greater control of ENSO on GWS across the USA (Kuss and Gurdak 2014) and the positive relationships between ENSO and TWS over Equatorial eastern Africa (Anyah et al. 2018) are also found. Besides, there are large COMMON-dominated areas with positive/negative correlations in western/eastern Australia, which is similar to the seesaw phenomenon described by Chen et al. (2021a) (i.e., eastern Australia is gaining water, while western Australia is losing water, and vice versa). The small ENSO+PDO-dominated areas also support the conclusion in Guo et al. (2021).

There are also some findings in our results that have not been reported in previous studies. For example, Liu et al. (2020) found that ENSO, AO and NAO are the three dominant factors controlling the variations of TWS over Asia and Eastern Europe. However, AO and NAO dominate only a small fraction of areas in our work. Several reasons are responsible for these differences. First, different components of TWS (i.e., WSCs) are considered in this study, while Liu et al. (2020) only considered TWS as a whole and also suggested a divergent response of hydrological components to TCs. Second, more regional TCs used in Liu et al. (2020) may mask the influences of six dominant TCs used in this study. Third, a newer version of JPL mascons is used in our studies, which provides more accurate TWS data. Fourth, moving average is not applied to smooth the residual series in Liu et al. (2020); hence some high-frequency noise may affect the results. Besides, some other factors can also lead to different results. For example, focusing on TCs with anomaly centers close to the areas of interest, some studies (Han et al. 2019; Yao 2017; Zhang et al. 2015) neglect the influences of TCs with anomaly centers far away from the study areas, which may be the dominant factors based on our results. Limiting the number of lag months to a narrow range (Guo et al. 2021) could omit the second peak of lag distribution, although their first peak of lags is close to five months. In some studies, detrend and deseasonalization are not applied in the data-processing steps (e.g.,

Anyah et al. 2018; Han et al. 2019; Soni and Syed 2015)—their results are prone to be affected by the long-term and seasonal signals of irrelevant factors (i.e., climate changes and human activities).

Uncertainty and Limitation

We note that there are sources of uncertainties and limitations of the current study. First, we acknowledge uncertainties (e.g., model structure error) in the estimates of the WSCs, especially for ones derived from global hydrological models (Scanlon et al. 2018). In situ observations of WSCs with high accuracy are expected to be used in future studies. The data from various sources might also be fused for quantifying the uncertainty of results (e.g., via the methods of difference (Fig. S2 in the Supplementary Material) and three-cornered hat (Long et al. 2017)).

Intermediate variables (e.g., precipitation (Zhang et al. 2019) and evapotranspiration) and attributions of areas like vegetation coverage can be used to analyze mechanisms of TC influences on WSC variability. The impact of sunspot activities on TCs and WSCs (Han et al. 2019) should be further investigated. The relatively short data duration in this study (i.e., 15 years) limits its utility to understand longer-term TC-WSC relationships and their changes over time, e.g., there are only few phase changes of AMO during the study period.

As for the multi-period analysis, the moving average method can provide only an approximation to the real-world situation (Hassani et al. 2013) due to its assumption on the stationarity for the data, linearity for the model and normality for the residuals. Therefore, a method that does not depend on these assumptions, such as singular spectrum analysis, could be beneficial for further analyses (Colebrook 1978).

Conclusions

In this study, we systematically analyze the relationships between TCs and WSCs using cross-correlation analysis. WSC residuals are derived via the STL method and then filtered via the moving average method with different time windows. The influence of the various independent features of TCs is also revealed via the ICA method. The major conclusions drawn from this study are summarized as follows:

1. A yearly moving average is appropriate for constraining high-frequency noises and retaining informative fluctuations of WSC signals. The areas of dominant TWS and GWS are mainly in the low- or mid-latitude. Tropical and subtropical regions have the strongest correlations and a relatively small lag as for the response of WSCs to TCs. The areas dominated by IOD mainly distribute on Indian Ocean rim regions.

2. TWS and GWS are the two most dominant WSCs while ENSO and AMO are the two most dominant TCs. The lags have two modes, the more significant of which is approximately 5 months. The negative connections are generally stronger than the

positive connections. The WSCs at relatively shallow depths, which are generally affected by many large-lag controls from TCs, tend to be dominated by the TCs with many high-frequency components that are prone to having a relatively faster WSC response.

3. There are four significant ICs among the six TCs, which are, respectively, highly correlated with (i) ENSO and PDO, (ii) NAO and AO and AMO, (iii) IOD, (iv) all TCs, among which the fourth IC has the largest dominated areas and show the strongest links for controlling WSC variations. Compared with the analysis based on TCs, TC ICs generally have stronger hysteresis and more negative connections on WSCs.

Availability of data and material

Data will be made available on request.

Abbreviations

AMO:

Atlantic Multidecadal Oscillation

AO:

Arctic Oscillation

CLSM:

Catchment Land Surface Model

ENSO:

El Niño-Southern Oscillation

GRACE:

Gravity Recovery And Climate Experiment

GWS:

Groundwater Storage

IC:

Independent Components

ICA:

Independent Component Analysis

IOD:

Indian Ocean Dipole

ITCZ:

Intertropical Convergence Zone

JPL:

Jet Propulsion Laboratory

MEI:

Multivariate Enso Index

NAO:

North Atlantic Oscillation

NOAA:

National Oceanic and Atmospheric Administration

PCW:

Plant Canopy Water

PDO:

Pacific Decadal Oscillation

RZSM:

Root Zone Soil Moisture

SnWS:

Snow Water Storage

STL:

Seasonal-Trend Decomposition By Loess

SWS:

Surface Water Storage

TC:

Teleconnection

TWS:

Terrestrial Water Storage

WGHM:

Watergap Global Hydrology Model

WSC:

Water Storage Component

References

Anyah, R. O., Forootan, E., Awange, J. L., & Khaki, M. (2018). Understanding linkages between global climate indices and terrestrial water storage changes over Africa using GRACE products. Science of the Total Environment, 635, 1405–1416. https://doi.org/10.1016/j.scitotenv.2018.04.159

Banerjee, C., & Kumar, D. N. (2018). Analyzing Large-Scale Hydrologic Processes Using GRACE and Hydrometeorological Datasets. Water Resources Management, 32(13), 4409–4423. https://doi.org/10.1007/s11269-018-2070-x

Chen, A., Guan, H., & Batelaan, O. (2021a). Seesaw terrestrial wetting and drying between eastern and western Australia. Earth's Future, 9(5), e2020EF001893. https://doi.org/10.31219/osf.io/qz3pe

Chen, H., Teegavarapu, R. S. V., & Xu, Y. P. (2021b). Oceanic-Atmospheric Variability Influences on Baseflows in the Continental United States. Water Resources Management, 35(9), 3005–3022. https://doi.org/10.1007/s11269-021-02884-6

Cleveland, R. B., Cleveland, W. S., & Mcrae, J. E. (1990). STL: A Seasonal-Trend Decomposition Procedure Based on Loess. J. Off. Stat., 6, 3–73.

Colebrook, J. M. (1978). Continuous Plankton Records: zooplankton and environment, north-east Atlantic and North sea, 1948-1975. Oceanologica Acta, 1(1), 9–23. Retrieved from http://archimer.ifremer.fr/doc/00123/23405/21232.pdf

García-García, D., Ummenhofer, C. C., & Zlotnicki, V. (2011). Australian water mass variations from GRACE data linked to Indo-Pacific climate variability. Remote Sensing of Environment, 115(9), 2175–2183. https://doi.org/10.1016/j.rse.2011.04.007

Girishkumar, M. S., Thanga Prakash, V. P., & Ravichandran, M. (2015). Influence of Pacific Decadal Oscillation on the relationship between ENSO and tropical cyclone activity in the Bay of Bengal during October–December. Climate Dynamics, 44(11–12), 3469–3479. https://doi.org/10.1007/s00382-014-2282-6

Guo, L., Li, T., Chen, D., Liu, J., He, B., & Zhang, Y. (2021). Links between global terrestrial water storage and large-scale modes of climatic variability. Journal of Hydrology, 598(May), 126419. https://doi.org/10.1016/j.jhydrol.2021.126419

Guo, Y., Huang, S., Huang, Q., Wang, H., Fang, W., Yang, Y., & Wang, L. (2019). Assessing socioeconomic drought based on an improved Multivariate Standardized Reliability and Resilience Index. Journal of Hydrology, 568(August), 904–918. https://doi.org/10.1016/j.jhydrol.2018.11.055

Han, Z., Huang, S., Huang, Q., Leng, G., Wang, H., He, L., et al. (2019). Assessing GRACE-based terrestrial water storage anomalies dynamics at multi-timescales and their correlations with teleconnection factors in Yunnan Province, China. Journal of Hydrology, 574(January), 836–850. https://doi.org/10.1016/j.jhydrol.2019.04.093

Hassani, H., Heravi, S., & Zhigljavsky, A. (2013). Forecasting UK industrial production with multivariate singular spectrum analysis. Journal of Forecasting, 32(5), 395–408. https://doi.org/10.1002/for.2244

Hu, B., Wang, L., Li, X., Zhou, J., & Pan, Y. (2021). Divergent Changes in Terrestrial Water Storage Across Global Arid and Humid Basins. Geophysical Research Letters, 48(1), 1–11. https://doi.org/10.1029/2020GL091069

Humphrey, V., Zscheischler, J., Ciais, P., Gudmundsson, L., Sitch, S., & Seneviratne, S. I. (2018). Sensitivity of atmospheric CO2 growth rate to observed changes in terrestrial water storage. Nature, 560(7720), 628–631. https://doi.org/10.1038/s41586-018-0424-4

Hyvärinen, A., & Oja, E. (2000). Independent component analysis: Algorithms and applications. Neural Networks, 13(4–5), 411–430. https://doi.org/10.1016/S0893-6080(00)00026-5

Hyvärinen, Aapo, Karhunen, J., & Oja, E. (2001). Independent Component Analysis. Wiley-Interscience. https://doi.org/10.1016/b978-0-444-64165-6.02006-1

Kennedy, A. M., Garen, D. C., & Koch, R. W. (2009). The association between climate teleconnection indices and Upper Klamath seasonal streamflow: Trans-Niño Index. Hydrological Processes, 23, 973–984. https://doi.org/10.1002/hyp

Krishan, G., Lohani, A. K., Rao, M. S., & Kumar, C. P. (2014). Prioritization of groundwater monitoring sites using cross-correlation analysis. NDCWWC Journal (A Half Yearly Journal of New Delhi Centre of WWC), 3, 28–31.

Kuss, A. J. M., & Gurdak, J. J. (2014). Groundwater level response in U.S. principal aquifers to ENSO, NAO, PDO, and AMO. Journal of Hydrology, 519, 1939–1952. https://doi.org/10.1016/j.jhydrol.2014.09.069

Liu, X., Feng, X., Ciais, P., & Fu, B. (2020). Widespread decline in terrestrial water storage and its link to teleconnections across Asia and eastern Europe. Hydrology and Earth System Sciences, 24(7), 3663–3676. https://doi.org/10.5194/hess-24-3663-2020

Long, D., Yang, Y., Wada, Y., Hong, Y., Liang, W., Chen, Y., et al. (2015). Deriving scaling factors using a global hydrological model to restore GRACE total water storage changes for China's Yangtze River Basin. Remote Sensing of Environment, 168, 177–193. https://doi.org/10.1016/j.rse.2015.07.003

Long, D., Pan, Y., Zhou, J., Chen, Y., Hou, X., Hong, Y., et al. (2017). Global analysis of spatiotemporal variability in merged total water storage changes using multiple GRACE products and global hydrological models. Remote Sensing of Environment, 192, 198–216. https://doi.org/10.1016/j.rse.2017.02.011

Müller Schmied, H., Cáceres, D., Eisner, S., Flörke, M., Herbert, C., Niemann, C., et al. (2020). The global water resources and use model WaterGAP v2.2d: Model description and evaluation. Geoscientific Model Development, 14, 1037–1079. https://doi.org/10.5194/gmd-2020-225

Ndehedehe, C. E., Awange, J. L., Kuhn, M., Agutu, N. O., & Fukuda, Y. (2017). Climate teleconnections influence on West Africa's terrestrial water storage. Hydrological Processes, 31(18), 3206–3224. https://doi.org/10.1002/hyp.11237

Ni, S., Chen, J., Wilson, C. R., Li, J., Hu, X., & Fu, R. (2018). Global Terrestrial Water Storage Changes and Connections to ENSO Events. Surveys in Geophysics, 39(1), 1–22. https://doi.org/10.1007/s10712-017-9421-7

Nie, N., Zhang, W., Chen, H., & Guo, H. (2018). A Global Hydrological Drought Index Dataset Based on Gravity Recovery and Climate Experiment (GRACE) Data. Water Resources Management, 32(4), 1275–1290. https://doi.org/10.1007/s11269-017-1869-1

Oñate-valdivieso, F., Uchuari, V., & Oñate-paladines, A. (2020). Large-Scale Climate Variability Patterns and Drought: A Case of Study in South – America. Water Resources Management, 34, 2061–2079.

Phillips, T., Nerem, R. S., Fox-Kemper, B., Famiglietti, J. S., & Rajagopalan, B. (2012). The influence of ENSO on global terrestrial water storage using GRACE. Geophysical Research Letters, 39(16), 1–7. https://doi.org/10.1029/2012GL052495

Qian, C., Yu, J. Y., & Chen, G. (2014). Decadal summer drought frequency in China: The increasing influence of the Atlantic Multi-decadal Oscillation. Environmental Research Letters, 9(12). https://doi.org/10.1088/1748-9326/9/12/124004

Runge, J., Nowack, P., Kretschmer, M., Flaxman, S., & Sejdinovic, D. (2019). Detecting causal associations in large nonlinear time series datasets. Science Advances, 11(5), eaau4996–eaau4996.

Saji, N. H., & Yamagata, T. (2003). Possible impacts of Indian Ocean Dipole mode events on global climate. Climate Research, 25(2), 151–169. https://doi.org/10.3354/cr025151

Scanlon, B. R., Zhang, Z., Save, H., Wiese, D. N., Landerer, F. W., Long, D., et al. (2016). Global evaluation of new GRACE mascon products for hydrologic applications. Water Resources Research, 12, 9412–9429. https://doi.org/10.1111/j.1752-1688.1969.tb04897.x

Scanlon, B. R., Zhang, Z., Save, H., Sun, A. Y., Müller Schmied, H., van Beek, L. P. H., et al. (2018). Global models underestimate large decadal declining and rising water storage trends relative to GRACE satellite data. Proceedings of the National Academy of Sciences, 115, E1080–E1089. https://doi.org/10.1073/pnas.1704665115

Soni, A., & Syed, T. H. (2015). Diagnosing Land Water Storage Variations in Major Indian River Basins using GRACE observations. Global and Planetary Change, 133, 263–271. https://doi.org/10.1016/j.gloplacha.2015.09.007

Sun, Z., Zhu, X., Pan, Y., Zhang, J., & Liu, X. (2018). Drought evaluation using the GRACE terrestrial water storage deficit over the Yangtze River Basin, China. Science of the Total Environment, 634, 727–738. https://doi.org/10.1016/j.scitotenv.2018.03.292

Sun, Z., Long, D., Yang, W., Li, X., & Pan, Y. (2020). Reconstruction of GRACE Data on Changes in Total Water Storage Over the Global Land Surface and 60 Basins. Water Resources Research, 56(4), 1–21. https://doi.org/10.1029/2019WR026250

Thomas, B. F., & Famiglietti, J. S. (2019). Identifying Climate-Induced Groundwater Depletion in GRACE Observations. Scientific Reports, 9(1), 1–9. https://doi.org/10.1038/s41598-019-40155-y

Wang, J., Song, C., Reager, J. T., Yao, F., Famiglietti, J. S., Sheng, Y., et al. (2018). Recent global decline in endorheic basin water storages. Nature Geoscience, 11(12), 926–932. https://doi.org/10.1038/s41561-018-0265-7

Xia, Y., Hao, Z., Shi, C., Li, Y., Meng, J., Xu, T., et al. (2019). Regional and Global Land Data Assimilation Systems: Innovations, Challenges, and Prospects. Journal of Meteorological Research, 33(2), 159–189. https://doi.org/10.1007/s13351-019-8172-4

Yang, P., Xia, J., Zhan, C., Qiao, Y., & Wang, Y. (2017). Monitoring the spatio-temporal changes of terrestrial water storage using GRACE data in the Tarim River basin between 2002 and 2015. Science of the Total Environment, 595, 218–228. https://doi.org/10.1016/j.scitotenv.2017.03.268

Yao, Z. (2017). Natural- and Human-Induced Impacts on Regional Terrestrial Water Storage Changes from GRACE and Hydro-Meteorological Data. Doctoral dissertation, Wuhan: Wuhan University (in Chinese with English abstract).

Zhang, Y., He, B. I. N., Guo, L., & Liu, D. (2019). Differences in response of terrestrial water storage components to precipitation over 168 global river basins. Journal of Hydrometeorology, 20(9), 1981–1999. https://doi.org/10.1175/JHM-D-18-0253.1

Zhang, Z., Chao, B. F., Chen, J., & Wilson, C. R. (2015). Terrestrial water storage anomalies of yangtze river basin droughts observed by GRACE and connections with ENSO. Global and Planetary Change, 126, 35–45. https://doi.org/10.1016/j.gloplacha.2015.01.002